PERGAMON

International Journal of Solids and Structures 37 (2000) 7743–7757

INTERNATIONAL JOURNAL OF SOLIDS and STRUCTURES

www.elsevier.com/locate/ijsolstr

Interaction between an interface crack and subinterface microcracks in metal/piezoelectric bimaterials

Wen-Ye Tian *, Yi-Heng Chen

School of Civil Engineering and Mechanics, Xi'an Jiaotong University, Xi'an 710049, People's Republic of China

Received 6 October 1999; in revised form 16 February 2000

Abstract

A semi-infinite interface macrocrack interacting with multiple oriented subinterface microcracks in the process zone near the macrocrack tip in metal/piezoelectric bimaterials is studied. After deriving the elementary solutions for a semi-infinite interface crack and a special subinterface crack under various loading conditions, the present interaction problem is deduced to a system of integral equations with the aid of the pseudo-traction-electric-displacement method. The integral equations are then solved numerically by using the Chebyshev numerical integration technique. After doing so, the variable tendencies of the stress intensity factors at the interface macrocrack tip versus the location angle and the orientation angle of the subinterface cracks, and the distance between the interface crack tip and the center of the subinterface microcrack are derived and discussed. The numerical results are shown in the figures. Detailed comparisons between the results under the compound mechanical-electric loading conditions and those derived under purely mechanical loading conditions are performed. Some conclusions are given which are certain to be useful for investigating the microcrack shielding problems in metal/piezoelectric bimaterials.

Keywords: Interaction; Interface macrocrack; Subinterface microcrack; Metal/piezoelectric bimaterials

1. Introduction

With the rapid development of modern industry, piezoelectric materials are more and more widely used in smart materials and structures such as actuators, sensors and transducers. Generally speaking, piezoelectric materials are ceramics that are manufactured by using conventional ceramic manufacturing processes with high temperature and strong electric field. They show brittle nature and are liable to develop critical cracks under stress concentrating or cooling conditions. On the other hand, in practical engineering, piezoelectric ceramics are usually bonded with or embedded in metal or other kinds of materials to construct a variety of special functional components. Hence, during the manufacturing, maintenance and service of these intelligent components, macrocracks are often formed on interface of metal and piezoelectric phases due to impact, cooling or other unexpected reasons. Now, crack is one of the main damage sources of such kinds of

* Corresponding author.

0020-7683/00/$ - see front matter
PII: S0020-7683(00)00110-4

smart materials, and their low tolerance to interface damage and microdefects has received much attention in the last twenty years. A large number of investigations on this topic have been done and a great progress has been made. For example, Parton (1976) has considered the problem of a finite crack at the interface between two piezoelectric materials subjected to a far field uniform tension; Sosa and Pak (1990) developed a three-dimensional solution for a semi-infinite crack in a piezoelectric material; Shindo and Ozawa (1990) analyzed cracks in piezoelectric layers using integral equation methods; Kuo and Barnett (1991) carried out an asymptotic crack tip analysis and found various singularities depending on the crack face boundary conditions; Pak (1992) investigated the electroelastic field and the energy release rate for a finite crack by way of the method of distributed dislocations and electric dipoles; Sosa (1992) obtained the asymptotic expressions for the electromechanical fields in the vicinity of a crack; Suo et al. (1992) solved the boundary value problem of electroelastic materials with interface cracks. More recently, Park and Sun (1995a,b) and Park and Carman (1997) studied the two-dimensional problems for an elliptic hole or crack in piezoelectric materials, and they defined two kinds of intensity factors, i.e., the Mode I and Mode II stress intensity factors (SIFs) and the electric displacement intensity factor (EDIF). However, on the whole, most of the above studies concentrated on the singularities at the tips of a crack, while little effort has been done in the interaction problem between an interface crack and subinterface cracks in metal/piezoelectric bimaterials. Especially, the microcrack shielding problems and the influence of the electric loading on the shielding effect in metal/piezoelectric bimaterials are still obsure for us and worthy of investigation.

The objective of the present work is to investigate the interaction between a semi-infinite interface macrocrack and multiple subinterface microcracks in the near tip process zone in metal/piezoelectric bimaterials. In Section 2, the fundamental solutions of a semi-infinite interface crack and a special subinterface crack subjected to three kinds of loadings are given, respectively. In Section 3, a pseudo-traction-electric-displacement method (PTEDM), which is motivated by the well-known pseudo-traction method (PTM) (Horii and Nemat-Nasser, 1985, 1987), is proposed to solve the present macrocrack–microcrack interaction problem which can be reduced to a system of integral equations. Using the Chebyshev numerical integration (Chen and Hasebe, 1994), the integral equations can be solved numerically. In Section 4, numerical results of the Mode I stress intensity factor for a special dissimilar piezoelectric material, i.e., Cu/PZT-4, are calculated and shown in figures, in which three kinds of remote loading conditions are preferred for making necessary comparisons. First of them is the compound mechanical-positive-electric loading, the second is the purely mechanical loading, while the third is the compound mechanical-negative-electric loading. Moreover, a detailed discussion about the macrocrack–microcrack interaction behavior is also performed in the same section.

2. Fundamental formula and fundamental solutions

Consider an infinite piezoelectric bimaterial plate, where material 1 and material 2 occupy the upper and the lower half-planes, respectively (Fig. 1).

In a linear piezoelectric medium, the elastic and electric field equations can be written as

$$\begin{aligned} &\sigma_{ij} = c_{ijkl}u_{k,l} + e_{lij}\phi_{,l}, \qquad D_i = e_{ikl}u_{k,l} - \varepsilon_{il}\phi_{,l}, \\ &\sigma_{ij,i} = 0, \qquad D_{i,i} = 0, \qquad E_l = -\phi_{,l}, \end{aligned} \tag{1}$$

where $\sigma_{ij}, u_i, D_i, E_i$ and ϕ are stress, displacement, electric displacement, electric fields and electric potential, respectively. c_{ijkl}, e_{ijk}, and ε_{il} are the corresponding elastic, piezoelectric, and dielectric constants, respectively.

It has been shown by Suo et al. (1992) that for a two-dimensional problem, the electroelastic field can be represented in terms of four functions $f_1(z_1)$, $f_2(z_2)$, $f_3(z_3)$, and $f_4(z_4)$, each of which is holomorphic in its

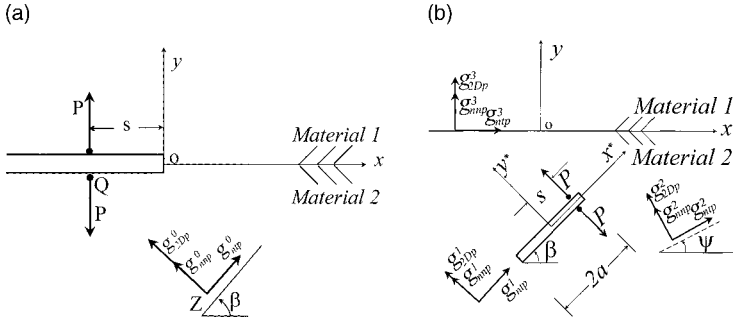

Fig. 1. (a) An interface macrocrack under concentrated normal tractions P and (b) a subinterface crack under concentrated normal tractions P.

argument $z_j = x + \mu_j y$. The representations for displacement u_r, electric potential ϕ, stresses σ_{ij}, and electric displacement D_i are

$$\begin{aligned} \{u_r, \phi\} &= 2\mathrm{Re}\sum_{\alpha=1}^{4}\mathbf{a}_\alpha \mathbf{f}_\alpha(z_\alpha), \\ \{\sigma_{2j}, D_2\} &= 2\mathrm{Re}\sum_{\alpha=1}^{4}\mathbf{b}_\alpha \mathbf{f}'_\alpha(z_\alpha), \\ \{\sigma_{1j}, D_1\} &= -2\mathrm{Re}\sum_{\alpha=1}^{4}\mathbf{b}_\alpha \mu_\alpha \mathbf{f}'_\alpha(z_\alpha). \end{aligned} \tag{2}$$

Here, $(\ )'$ is designated as the derivative with respect to the associated arguments, $\mathbf{a}$ and μ satisfy the following equation:

$$\{\mathbf{Q} + \mu(\mathbf{R} + \mathbf{R}^{\mathrm{T}}) + \mu^2\mathbf{T}\}\mathbf{a} = 0, \tag{3}$$

where $\mathbf{a} = (a_1, a_2, a_3, a_4)^{\mathrm{T}}$, and $\mathbf{Q}$, $\mathbf{R}$, and $\mathbf{T}$ are 4×4 matrices defined as

$$\mathbf{Q} = \begin{bmatrix} c_{i1k1} & e_{1i1} \\ e^{\mathrm{T}}_{1k1} & -\varepsilon_{11} \end{bmatrix}, \qquad \mathbf{R} = \begin{bmatrix} c_{i1k2} & e_{2i1} \\ e^{\mathrm{T}}_{1k2} & -\varepsilon_{12} \end{bmatrix}, \qquad \mathbf{T} = \begin{bmatrix} c_{i2k2} & e_{2i2} \\ e^{\mathrm{T}}_{2k2} & -\varepsilon_{22} \end{bmatrix}.$$

In order to obtain a nontrivial solution for Eq. (3), it is required that

$$\left\|\mathbf{Q} + \mu(\mathbf{R} + \mathbf{R}^{\mathrm{T}}) + \mu^2\mathbf{T}\right\| = 0. \tag{4}$$

The left-hand side of Eq. (4) is an eight-order polynomial in μ. Suo et al. (1992) showed that Eq. (4) has no real roots. Hence the eight eigenvalues form four conjugate pairs, i.e., μ_α and $\overline{\mu}_\alpha$ ($\mu_{\alpha+4} = \overline{\mu}_\alpha$, $\alpha = 1, 2, 3, 4$), where μ_α ($\alpha = 1, 2, 3, 4$) is assumed to have a positive imaginary part. Corresponding to each root, μ_α or $\overline{\mu}_\alpha$, there is a complex eigenvector $\mathbf{a}_\alpha$ and $\overline{\mathbf{a}}_\alpha$($\mathbf{a}_{\alpha+4} = \overline{\mathbf{a}}_\alpha$, $\alpha = 1, 2, 3, 4$). Moreover, the auxiliary vector $\mathbf{b}$ is

$$\mathbf{b} = (\mathbf{R}^{\mathrm{T}} + \mu\mathbf{T})\mathbf{a} = -\frac{1}{\mu}(\mathbf{Q} + \mu\mathbf{R})\mathbf{a}. \tag{5}$$

The two 4×4 matrices $\mathbf{A}$ and $\mathbf{L}$ are defined as

$$\mathbf{A} = [\mathbf{a}_1, \mathbf{a}_2, \mathbf{a}_3, \mathbf{a}_4], \qquad \mathbf{L} = [\mathbf{b}_1, \mathbf{b}_2, \mathbf{b}_3, \mathbf{b}_4]. \tag{6}$$

Suo et al. (1992) showed that $\mathbf{A}$ and $\mathbf{L}$ are nonsingular.

Let us define

$$\mathbf{Y} = i\mathbf{A}\mathbf{L}^{-1}. \tag{7}$$

A bimaterial matrix is defined as

$$\mathbf{H} = \mathbf{Y}^{\mathrm{U}} + \overline{\mathbf{Y}}^{\mathrm{L}}. \tag{8}$$

Here and throughout the paper, an overbar denotes the complex conjugation, and the terms U and L attached to matrices and vectors are reserved exclusively to indicate the upper material and the lower material, respectively.

Furthermore, Suo et al. (1992) defined the following function vector $\mathbf{f}(z)$:

$$\mathbf{f}(z) = [f_1(z), f_2(z), f_3(z), f_4(z)]^{\mathrm{T}}, \tag{9}$$

where the argument has the generic form $z = x + \mu y$.

Once the solution of $\mathbf{f}(z)$ is derived for a given boundary value problem, each component function to calculate the corresponding elastic field could then be evaluated from Eq. (2). Moreover, the set of vectors along the x-axis is given as

$$\begin{aligned} \mathbf{u}_x &= \{u_j(x,0), \phi\} = \mathbf{A}\mathbf{f}(x) + \overline{\mathbf{A}}\bar{\mathbf{f}}(x), \\ \mathbf{t}(x) &= \{\sigma_{2j}(x,0), D_2\} = \mathbf{L}\mathbf{f}'(x) + \overline{\mathbf{L}}\bar{\mathbf{f}}'(x) \qquad (j = 1,2,3). \end{aligned} \tag{10}$$

2.1. Fundamental solutions for a semi-infinite interface crack

Assume that the origin of the global system is located at the semi-infinite interface crack tip and the x-coordinate is along the interface, while the y-coordinate is perpendicular to the interface (Fig. 1(a)).

According to the continuous condition of the traction and the electric displacement across the whole x-axis, there is a relation between the upper boundary values and the lower boundary values denoted by the terms U and L as

$$\mathbf{L}^{\mathrm{U}}\mathbf{f}'^{\mathrm{U}}(x) + \overline{\mathbf{L}}^{\mathrm{U}}\bar{\mathbf{f}}'^{\mathrm{U}}(x) = \mathbf{L}^{\mathrm{L}}\mathbf{f}'^{\mathrm{L}}(x) + \overline{\mathbf{L}}^{\mathrm{L}}\bar{\mathbf{f}}'^{\mathrm{L}}(x). \tag{11}$$

For facilitating the analytic continuation, Eq. (11) is rearranged as

$$\mathbf{L}^{\mathrm{U}}\mathbf{f}'^{\mathrm{U}}(x) - \overline{\mathbf{L}}^{\mathrm{L}}\bar{\mathbf{f}}'^{\mathrm{L}}(x) = \mathbf{L}^{\mathrm{L}}\mathbf{f}'^{\mathrm{L}}(x) - \overline{\mathbf{L}}^{\mathrm{U}}\bar{\mathbf{f}}'^{\mathrm{U}}(x). \tag{12}$$

By using the standard analytic continuity argument, it follows that

$$\mathbf{L}^{\mathrm{U}}\mathbf{f}'^{\mathrm{U}}(z) = \overline{\mathbf{L}}^{\mathrm{L}}\bar{\mathbf{f}}'^{\mathrm{L}}(z). \tag{13}$$

The displacement and the electric potential jump across the interface is

$$d(x) = u(x,0^+) - u(x,0^-). \tag{14}$$

With the aid of Eq. (13), a direct calculation gives

$$\mathbf{t}(x) = \mathbf{L}^{\mathrm{U}}\mathbf{f}'^{\mathrm{U}}(x) + \mathbf{L}^{\mathrm{L}}\mathbf{f}'^{\mathrm{L}}(x), \tag{15}$$

$$i\mathbf{d}'(x) = \mathbf{H}\mathbf{L}^{\mathrm{U}}\mathbf{f}'^{\mathrm{U}}(x) - \overline{\mathbf{H}}\mathbf{L}^{\mathrm{L}}\mathbf{f}'^{\mathrm{L}}(x). \tag{16}$$

According to the continuity of the displacement and the electric potential across the bonded interface as inferred from Eq. (16), $\mathbf{L}^{\mathrm{U}}\mathbf{f}'^{\mathrm{U}}(x)$ and $\mathbf{L}^{\mathrm{L}}\mathbf{f}'^{\mathrm{L}}(x)$ can be analytically extended to the whole plane except on the crack line and satisfy

$$\mathbf{h}(z) = \mathbf{L}^{\mathrm{U}}\mathbf{f}'^{\mathrm{U}}(z) = \mathbf{H}^{-1}\overline{\mathbf{H}}\mathbf{L}^{\mathrm{L}}\mathbf{f}'^{\mathrm{L}}(z), \quad z \notin c, \tag{17}$$

where $\mathbf{h}(z)$ is introduced for convenience, c is denoted as the crack line. Hence, one can focus on $\mathbf{h}(z)$, and once $\mathbf{h}(z)$ is obtained, the full-field solution could be given by Eq. (17). In terms of $\mathbf{h}(z)$, the traction and the electric displacement (15) and displacement and electric potential jump (16) can be expressed as

$$\mathbf{t}(x) = \mathbf{h}^{+}(x) + \overline{\mathbf{H}}^{-1}\mathbf{H}\mathbf{h}^{-}(x), \tag{18}$$

$$i\mathbf{d}'(x) = \mathbf{H}[\mathbf{h}^{+}(x) - \mathbf{h}^{-}(x)]. \tag{19}$$

Now, consider the problem of a semi-infinite interface crack, the prescribed traction and electric displacement $\mathbf{t}_0(x)$ on the crack lines results in the following Hilbert problem:

$$\mathbf{h}^{+}(x) + \overline{\mathbf{H}}^{-1}\mathbf{H}\mathbf{h}^{-}(x) = \mathbf{t}_0(x), \quad x \in c, \tag{20}$$

its complete solution is

$$\mathbf{h}(z) = h_1(z)\mathbf{w}_1 + h_2(z)\overline{\mathbf{w}}_1 + h_3(z)\mathbf{w}_3 + h_4(z)\mathbf{w}_4, \tag{21}$$

where

$$\begin{aligned}
h_1(z) &= \frac{\chi(z)}{2\pi i}\int_c \frac{t_{01}(x)\,\mathrm{d}x}{\chi^{+}(x)(x-z)},\\
h_2(z) &= \frac{\bar{\chi}(z)}{2\pi i}\int_c \frac{\bar{t}_{01}(x)\,\mathrm{d}x}{\bar{\chi}^{+}(x)(x-z)},\\
h_3(z) &= \frac{\chi_3(z)}{2\pi i}\int_c \frac{t_{03}(x)\,\mathrm{d}x}{\chi_3^{+}(x)(x-z)},\\
h_4(z) &= \frac{\chi_4(z)}{2\pi i}\int_c \frac{t_{04}(x)\,\mathrm{d}x}{\chi_4^{+}(x)(x-z)},\\
\chi(z) &= z^{-1/2-i\varepsilon},\\
\chi_3(z) &= z^{-1/2+k},\\
\chi_4(z) &= z^{-1/2-k}.
\end{aligned} \tag{22}$$

Here, four eigenpairs $(\varepsilon, \mathbf{w}_1)$, $(-\varepsilon, \overline{\mathbf{w}}_1)$, $(-ik, \mathbf{w}_3)$ and $(ik, \mathbf{w}_4)$ satisfy the following equation:

$$\overline{\mathbf{H}}\mathbf{w} = \mathrm{e}^{2\pi\varepsilon}\mathbf{H}\mathbf{w}. \tag{23}$$

Then the stresses g^0_{nnp}, g^0_{ntp} and the electric displacement g^0_{2Dp} at a point z due to the normal concentrated traction P shown in Fig. 1(a) can be calculated by Eqs. (2), (17) and (20):

$$\begin{aligned}
g^0_{nnp} &= 2\mathrm{Re}\sum_{\alpha=1}^{4}\left[(-b_{1\alpha}\mu_\alpha \sin^2\beta + b_{2\alpha}\cos^2\beta - b_{1\alpha}\sin 2\beta)f'_\alpha(z_\alpha)\right],\\
g^0_{ntp} &= 2\mathrm{Re}\sum_{\alpha=1}^{4}\left[\left(\tfrac{1}{2}b_{1\alpha}\mu_\alpha \sin 2\beta + \tfrac{1}{2}b_{2\alpha}\sin 2\beta + b_{1\alpha}\cos 2\beta\right)f'_\alpha(z_\alpha)\right],\\
g^0_{2Dp} &= 2\mathrm{Re}\sum_{\alpha=1}^{4}\left[(b_{4\alpha}\mu_\alpha \sin\beta + b_{4\alpha}\cos\beta)f'_\alpha(z_\alpha)\right].
\end{aligned} \tag{24}$$

Similarly, the stresses g^0_{nnq}, g^0_{ntq} and the electric displacement g^0_{2Dq} at a point z due to the tangential concentrated traction Q, and the stresses g^0_{nnd}, g^0_{ntd} and the electric displacement g^0_{2Dd} at a point z due to the

concentrated electric displacement D_2 can also be calculated by Eqs. (2), (17) and (20), expressions of which are not listed here.

2.2. Fundamental solutions for a subinterface crack

Consider a subinterface crack of length $2a$ subjected to the concentrated normal traction P on the crack faces in an infinite dissimilar piezoelectric plane as shown in Fig. 1(b). With the aid of the idea of Suo (1990), fundamental solutions for the subinterface crack could be constructed from the corresponding solutions in a homogeneous piezoelectric plane $f_0(z)$ ($z = x + \mu y$), μ is the characteristic root of the homogeneous piezoelectric material.

$$\mathbf{f}(z) = \begin{cases} \mathbf{f}^1(z), & z \in \text{upper half plane or } y > 0, \\ \mathbf{f}^2(z) + \mathbf{f}_0(z), & z \in \text{lower half plane or } y < 0, \end{cases} \tag{25}$$

where $z = x + u_j y$ ($j = 1, 2, 3, 4$).

According to the continuity of tractions, electric displacements, displacements and electric potential across the interface, the potentials of the upper and the lower planes could be given as

$$\mathbf{f}^1(z) = \mathbf{L}^{\mathrm{U}^{-1}}\mathbf{H}^{-1}(\overline{\mathbf{Y}}^{\mathrm{L}} + \mathbf{Y}^{\mathrm{L}})\mathbf{L}^{\mathrm{L}}\mathbf{f}_0(z), \quad z \in \text{upper half plane}, \tag{26}$$

$$\mathbf{f}^2(z) = \overline{\mathbf{L}}^{\mathrm{L}^{-1}}\overline{\mathbf{H}}^{-1}(\overline{\mathbf{Y}}^{\mathrm{L}} - \overline{\mathbf{Y}}^{\mathrm{U}})\overline{\mathbf{L}}^{\mathrm{L}}\bar{\mathbf{f}}_0(z), \quad z \in \text{lower half plane}, \tag{27}$$

where the overbar denotes the complex conjugate, and the matrixes $\mathbf{L}^{\mathrm{U}}, \mathbf{L}^{\mathrm{L}}, \mathbf{H}, \mathbf{Y}^{\mathrm{U}}, \mathbf{Y}^{\mathrm{L}}$ are given in Eqs. (6)–(8).

By substituting Eqs. (26) and (27) into Eq. (25), the solution in the whole plane including two materials is then obtained. It should be emphasized that the complex variable z should be replaced by $z_j = x + \mu_j y$ when calculating the corresponding quantities via Eq. (2), respectively, for $\mathbf{f}(z)$ in Eq. (25).

Then, the stresses g^1_{nnp}, g^1_{ntp} and the electric displacement g^1_{2Dp} along crack line, the stresses g^2_{nnp}, g^2_{ntp} and the electric displacement g^2_{2Dp} along dashed line, and the stresses g^3_{nnp}, g^3_{ntp} and the electric displacement g^3_{2Dp} along the interface due to the normal concentrated traction P shown in Fig. 1(b) can be calculated by Eqs. (2) and (25):

$$\begin{aligned} g^1_{nnp} &= -P\delta(t-s) + 2\mathrm{Re}\sum_{\alpha=1}^{4}(-b_{1\alpha}\mu_\alpha \sin^2\beta + b_{2\alpha}\cos^2\beta - b_{1\alpha}\sin 2\beta)f'_\alpha(z_\alpha), \\ g^1_{ntp} &= \mathrm{Re}\sum_{\alpha=1}^{4}(b_{1\alpha}\mu_\alpha \sin 2\beta + b_{2\alpha}\sin 2\beta + 2b_{1\alpha}\cos 2\beta)f'_\alpha(z_\alpha), \\ g^1_{2Dp} &= 2\mathrm{Re}\sum_{\alpha=1}^{4}(b_{4\alpha}\mu_\alpha \sin\beta + b_{4\alpha}\cos\beta)f'_\alpha(z_\alpha), \end{aligned} \tag{28a}$$

$$\begin{aligned} g^2_{nnp} &= 2\mathrm{Re}\sum_{\alpha=1}^{4}(-b_{1\alpha}\mu_\alpha \sin^2\psi + b_{2\alpha}\cos^2\psi - b_{1\alpha}\sin 2\psi)f'_\alpha(z_\alpha), \\ g^2_{ntp} &= \mathrm{Re}\sum_{\alpha=1}^{4}(b_{1\alpha}\mu_\alpha \sin 2\psi + b_{2\alpha}\sin 2\psi + 2b_{1\alpha}\cos 2\psi)f'_\alpha(z_\alpha), \\ g^2_{2Dp} &= 2\mathrm{Re}\sum_{\alpha=1}^{4}(b_{4\alpha}\mu_\alpha \sin\psi + b_{4\alpha}\cos\psi)f'_\alpha(z_\alpha), \end{aligned} \tag{28b}$$

$$g^3_{nnp} = 2\mathrm{Re}\sum_{\alpha=1}^{4} b_{2\alpha} f'_\alpha(z_\alpha),$$
$$g^3_{ntp} = 2\mathrm{Re}\sum_{\alpha=1}^{4} b_{1\alpha} f'_\alpha(z_\alpha), \tag{28c}$$
$$g^3_{2Dp} = 2\mathrm{Re}\sum_{\alpha=1}^{4} b_{4\alpha} f'_\alpha(z_\alpha).$$

Similarly, the stresses g^1_{nnq}, g^1_{ntq} and the electric displacement g^1_{2Dq} along crack line, the stresses g^2_{nnq}, g^2_{ntq} and the electric displacement g^2_{2Dq} along dashed line, and the stresses g^3_{nnq}, g^3_{ntq} and the electric displacement g^3_{2Dq} along the interface due to the tangential concentrated traction Q, and the stresses g^1_{nnd}, g^1_{ntd} and the electric displacement g^1_{2Dd} along crack line, the stresses g^2_{nnd}, g^2_{ntd} and the electric displacement g^2_{2Dd} along dashed line, and the stresses g^3_{nnd}, g^3_{ntd} and the electric displacement g^3_{2Dd} along the interface due to the concentrated electric displacement D_2 can also be calculated by Eqs. (2) and (25), the expressions of which are not included in this paper.

2.3. Remote loading conditions

Consider a semi-infinite interface crack in an infinite dissimilar piezoelectric material loaded by the remote stress intensity factors K^∞_{I}, $K^\infty_{\mathrm{II}}, K^\infty_{\mathrm{III}}$ and the remote electric displacement intensity factor K^∞_{e}, the potential $\mathbf{h}(z)$ is

$$\mathbf{h}(z) = \frac{\mathrm{e}^{\pi\varepsilon} K z^{i\varepsilon}\mathbf{w}_1 + \mathrm{e}^{-\pi\varepsilon}\overline{K} z^{-i\varepsilon}\overline{\mathbf{w}}_1}{2\sqrt{2\pi z}\cosh\pi\varepsilon} + \frac{K^\infty_{\mathrm{III}} z^k \mathbf{w}_3 + K^\infty_{\mathrm{e}} z^{-k}\mathbf{w}_4}{2\sqrt{2\pi z}\cos\pi k}, \tag{29}$$

where $K = K^\infty_{\mathrm{I}} + iK^\infty_{\mathrm{II}}$, ε, k and $\mathbf{w}$ are given by Eq. (23). After substituting Eq. (29) into Eq. (17), the potentials for the two half-spaces could then be obtained. When calculating the field quantities via Eq. (2), one has to replace z by $z_j = x + \mu_j y$ respectively for each component of $f(z)$ in Eq. (17).

3. Pseudo-traction-electric-displacement method

The problem to be solved in this section is shown in Fig. 2, in which N arbitrarily located subinterface cracks are formed in the process zone near the interface macrocrack tip in a metal/piezoelectric bimaterial. Here, $2a_k$ and β_k denote the crack length and the oriented angle of the kth crack. The bimaterial is loaded by the remote stresses $K^\infty_{\mathrm{I}}, K^\infty_{\mathrm{II}}$ and the remote electric displacement K^∞_{e}. All crack faces are assumed to be traction-free and electric-charge-free. Using the PTEDM proposed by Chen and Han (1999a) in homogeneous piezoelectric materials, the present problem is divided into $N+2$ sub-problems (Fig. 2), each of which contains one single crack with unknown tractions and unknown electric displacement attached on both faces. Using the fundamental solutions mentioned above and the superimposing technique, the following Fredholm integral equations is reduced:

$$P_0(s) + \sum_{k=1}^{N}\int_{-a_k}^{a_k} P_k(t_k) g^3_{nnp}(t_k, s)\,\mathrm{d}t_k + \sum_{k=1}^{N}\int_{-a_k}^{a_k} Q_k(t_k) g^3_{tnq}(t_k, s)\,\mathrm{d}t_k + \sum_{k=1}^{N}\int_{-a_k}^{a_k} D_k(t_k) g^3_{nnd}(t_k, s)\,\mathrm{d}t_k = 0$$
$$(-\infty < s < 0), \tag{30a}$$

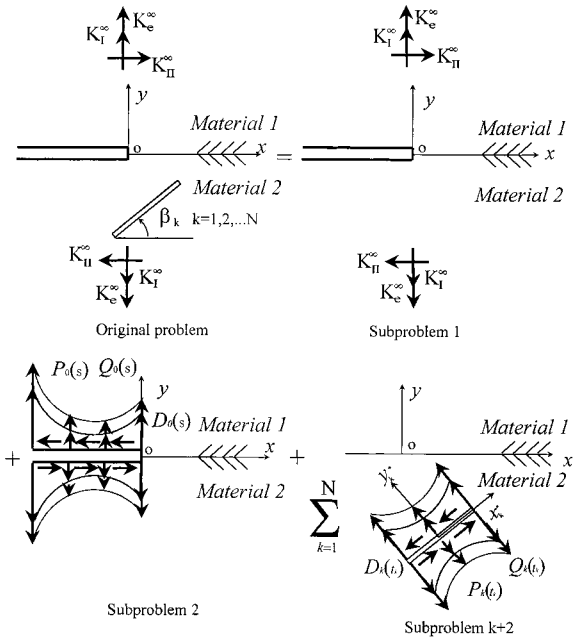

Fig. 2. Method of superimposing.

$$Q_0(s)+\sum_{k=1}^{N}\int_{-a_k}^{a_k}P_k(t_k)g^3_{ntp}(t_k,s)\,\mathrm{d}t_k+\sum_{k=1}^{N}\int_{-a_k}^{a_k}Q_k(t_k)g^3_{ttq}(t_k,s)\,\mathrm{d}t_k+\sum_{k=1}^{N}\int_{-a_k}^{a_k}D_k(t_k)g^3_{ttd}(t_k,s)\,\mathrm{d}t_k=0 \quad (-\infty<s<0), \tag{30b}$$

$$D_{20}(s)+\sum_{k=1}^{N}\int_{-a_k}^{a_k}P_k(s_k)g^3_{2Dp}(t_k,s)\,\mathrm{d}t_k+\sum_{k=1}^{N}\int_{-a_k}^{a_k}Q_k(t_k)g^3_{2Dq}(t_k,s)\,\mathrm{d}t_k+\sum_{k=1}^{N}\int_{-a_k}^{a_k}D_k(t_k)g^3_{2Dd}(t_k,s)\,\mathrm{d}t_k=0 \quad (-\infty<s<0), \tag{30c}$$

$$\begin{aligned}&\int_{-\infty}^{0}\left[g^0_{nnp}(s,t_k)P_0(s)+g^0_{nnq}(s,t_k)Q_0(s)+g^0_{nnd}(s,t_k)D_0(s)\right]\mathrm{d}s\ \int_{-a_k}^{a_k}\left[g^1_{nnp}(s_k,t_k)P_k(s_k)\right.\\&\left.+g^1_{nnq}(s_k,t_k)Q_k(s_k)+g^1_{nnd}(s_k,t_k)D_k(s_k)\right]\mathrm{d}s_k\ +\sum_{\substack{i=1\\i\neq k}}^{N}\int_{-a_i}^{a_i}\left[g^2_{nnp}(t_i,t_k)P_i(t_i)+g^2_{nnq}(t_i,t_k)Q_i(t_i)\right.\\&\left.+g^2_{nnd}(t_i,t_k)D_i(t_i)\right]\mathrm{d}t_i=p_k(t_k),\end{aligned} \tag{30d}$$

$$\begin{aligned}&\int_{-\infty}^{0}\left[g^0_{ntp}(s,t_k)P_0(s)+g^0_{ntq}(s,t_k)Q_0(s)+g^0_{ntd}(s,t_k)D_0(s)\right]\mathrm{d}s+\int_{-a_k}^{a_k}\left[g^1_{ntp}(s_k,t_k)P_k(s_k)\right.\\&\left.+g^1_{ntq}(s_k,t_k)Q_k(s_k)+g^1_{ntd}(s_k,t_k)D_k(s_k)\right]\mathrm{d}s_k\ +\sum_{\substack{i=1\\i\neq k}}^{N}\int_{-a_i}^{a_i}\left[g^2_{ntp}(t_i,t_k)P_i(t_i)+g^2_{ntq}(t_i,t_k)Q_i(t_i)\right.\\&\left.+g^2_{ntd}(t_i,t_k)D_i(t_i)\right]\mathrm{d}t_i=q_k(t_k),\end{aligned} \tag{30e}$$

$$\int_{-\infty}^{0}\left[g_{2Dp}^{0}(s,t_k)P_0(s)+g_{2Dq}^{0}(s,t_k)Q_0(s)+g_{2Dd}^{0}(s,t_k)D_0(s)\right]\mathrm{d}s+\int_{-a_k}^{a_k}\left[g_{2Dp}^{1}(s_k,t_k)P_k(s_k)\right.$$
$$\left.+g_{2Dq}^{1}(s_k,t_k)Q_k(s_k)+g_{2Dd}^{1}(s_k,t_k)D_k(s_k)\right]\mathrm{d}s_k+\sum_{\substack{i=1\\ i\neq k}}^{N}\int_{-a_i}^{a_i}\left[g_{2Dp}^{2}(t_i,t_k)P_i(t_i)+g_{2Dq}^{2}(t_i,t_k)Q_i(t_i)\right.$$
$$\left.+g_{2Dd}^{2}(t_i,t_k)D_i(t_i)\right]\mathrm{d}t_i=d_{2k}(t_k)$$
$$(-a_k<s_k<a_k,\ -a_k<t_k<a_k,\ k=1,2,\ldots,N), \tag{30f}$$

where $P_0(s)$, $Q_0(s)$, $P_k(s_k)$, $Q_k(s_k)$, $P_i(t_i)$, $Q_i(t_i)$, and $D_0(s)$, $D_k(t_k)$, $D_i(t_i)$ are the so-called pseudo-tractions and pseudo-electric-displacements to be determined, the thirty-six kernel functions g_{nnp}^{0}, g_{nnq}^{0}, g_{nnd}^{0}, g_{ntp}^{0}, g_{ntq}^{0}, g_{ntd}^{0}, g_{2Dp}^{0}, g_{2Dq}^{0}, g_{2Dd}^{0}, g_{nnp}^{1}, g_{nnq}^{1}, g_{nnd}^{1}, g_{nnp}^{2}, g_{nnq}^{2}, g_{nnd}^{2}, g_{ntp}^{1}, g_{ntq}^{1}, g_{ntd}^{1}, g_{ntp}^{2}, g_{ntq}^{2}, g_{ntd}^{2}, g_{2Dp}^{1}, g_{2Dq}^{1}, g_{2Dd}^{1}, g_{2Dq}^{2}, g_{2Dp}^{2}, g_{2Dd}^{2} g_{nnp}^{3}, g_{nnq}^{3}, g_{nnd}^{3}, g_{ntp}^{3}, g_{ntq}^{3}, g_{ntd}^{3}, g_{2Dp}^{3}, g_{2Dq}^{3}, and g_{2Dd}^{3} are given in Section 2. The subscripts, n, t, D, 0, k, and i indicate the normal quantities, the tangential quantities, the electric quantities, the interface macrocrack, the kth crack and the ith crack, respectively. The terms on the right-hand sides of Eqs. (30d)–(30f) $p_k(t_k)$, $q_k(t_k)$, and $d_{2k}(t_k)$ are the known stresses and the known electric displacement on the crack faces, respectively, induced from the remote loading conditions.

Using the Chebyshev numerical integration technique, the integral Eqs. (30a)–(30f) could be solved numerically for the unknown pseudo-tractions $P_k(s_k)$, $Q_k(s_k)$, and unknown pseudo-electric-displacement $D_k(t_k)$ $(k=0,1,2,\ldots,N)$. After doing so, the stress intensity factors $(K_{\mathrm{I}},K_{\mathrm{II}})$ and the electric displacement intensity factors (K_{e}) at the crack tips could be evaluated without any difficulty.

The stress intensity factor for the semi-infinite interface crack in dissimilar piezoelectric materials could be expressed as

$$K^{t}=K_{\mathrm{I}}^{t}+iK_{\mathrm{II}}^{t}=-(2/\pi)^{1/2}\cosh\pi\varepsilon\int_{-\infty}^{0}(-x)^{-1/2-i\varepsilon}t_{01}(x)\,\mathrm{d}x,$$
$$K_{\mathrm{e}}^{t}=-(2/\pi)^{1/2}\cos\pi k\int_{-\infty}^{0}(-x)^{-1/2+k}t_{04}(x)\,\mathrm{d}x. \tag{31}$$

The stress intensity factors for the kth subinterface crack are

$$K_{\mathrm{I}}^{\mathrm{R}}+iK_{\mathrm{II}}^{\mathrm{R}}=-(\pi a)^{-1/2}\int_{-a_k}^{a_k}\left(\frac{a_k+x_k}{a_k-x_k}\right)^{1/2}(P_k+iQ_k)\,\mathrm{d}x_k,$$
$$K_{\mathrm{e}}^{\mathrm{R}}=-(\pi a)^{-1/2}\int_{-a_k}^{a_k}\left(\frac{a_k+x_k}{a_k-x_k}\right)^{1/2}D_k\,\mathrm{d}x_k, \tag{32}$$

where the term R denotes the right crack tip, with an analogous expression at the left crack tip.

4. Numerical examples and discussion

Consider an infinite piezoelectric bimaterial plate containing an interface macrocrack and a subinterface microcrack of length $2a$ as shown in Fig. 3. r is the distance between the macrocrack tip and the center of the subinterface crack, θ is the angle between the r and the x-axis, β is the orientation angle of the subinterface crack. Take $r/a=1.3$, $\beta=0^{\circ}$ and let the same piezoelectric material (PZT-4) occupy the upper and lower half-spaces and the poling direction of the material is perpendicular to the macrocrack; thus, the present problem is reduced to a homogeneous problem whose solutions have been given by Chen and Han (1999b). Using the method established in this paper, the numerical results of the normalized Mode I stress

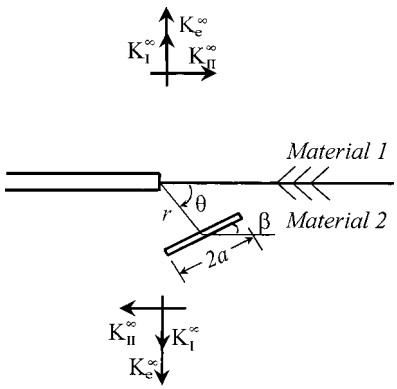

Fig. 3. An interface macrocrack and a subinterface microcrack.

intensity factor K_I^t/K_I^∞ at the macrocrack tip versus the location angle θ of the microcrack under three different loading conditions are calculated and listed in Table 1. Among the three kinds of loadings, the first is the compound mechanical-positive-electric loading ($K_I^\infty \neq 0, K_{II}^\infty = 0, K_e^\infty = 10^{-8} K_I^\infty CN^{-1}$), the second is the purely mechanical loading ($K_I^\infty \neq 0, K_{II}^\infty = 0, K_e^\infty = 0$), and the third is the compound mechanical-negative-electric loading ($K_I^\infty \neq 0, K_{II}^\infty = 0, K_e^\infty = -10^{-8} K_I^\infty CN^{-1}$). From Table 1, it is found that the numerical results obtained in this paper well agree with those given by Chen and Han (1999b). The above comparison results fully demonstrate the reliability of the numerical computing scheme proposed in this paper.

The following results are gained by using a special kind of material combination, Cu/PZT-4, the material constants are listed in Tables 2 and 3. Here, it should be noted that the brittle piezoelectric materials always occupy the lower half-plane, so it is more possible for cracks to appear in material 2, namely, subinterface cracks. Also, the plane strain is considered.

First, consider an interface macrocrack and a parallel subinterface microcrack of length $2a$ as shown in Fig. 3 ($\beta = 0°$). Under the three kinds of loading conditions mentioned above, taking $r/a = 1.2, 1.5$, and

Table 1
The values of K_I^t/K_I^∞ for the homogeneous piezoelectric material (PZT-4)

θ (deg)	Numerical values		
	$K_I^\infty \neq 0,\ K_{II}^\infty = 0,$ $K_e^\infty = 10^{-8} K_I^\infty CN^{-1}$	$K_I^\infty \neq 0,\ K_{II}^\infty = 0,$ $K_e^\infty = 0$	$K_I^\infty \neq 0,\ K_{II}^\infty = 0,$ $K_e^\infty = -10^{-8} K_I^\infty CN^{-1}$
17	1.3676	1.3353	1.3030
51	1.0761	1.0499	1.0238
68	0.9384	0.9530	0.9676
136	0.8183	0.8283	0.8385
153	0.9066	0.8765	0.8464

Table 2
Material constants of the PTZ-4 ceramic

C_{11}	C_{12}	C_{13}	C_{33}	C_{44}	e_{31}	e_{33}	e_{15}	w_{11}	w_{33}
1.4020	0.7892	0.7565	1.1577	0.2525	−5.2677	15.4455	12.0000	0.6359	0.5523

The C values are expressed in $N/m^2 \times 10^{11}$, e values in C/m^2 and w values in $C/V\,m \times 10^{-8}$.

Table 3
Material constants of Cu

Shear modulus ($N/m^2 \times 10^{11}$)	Poisson's ratio
0.478	0.345

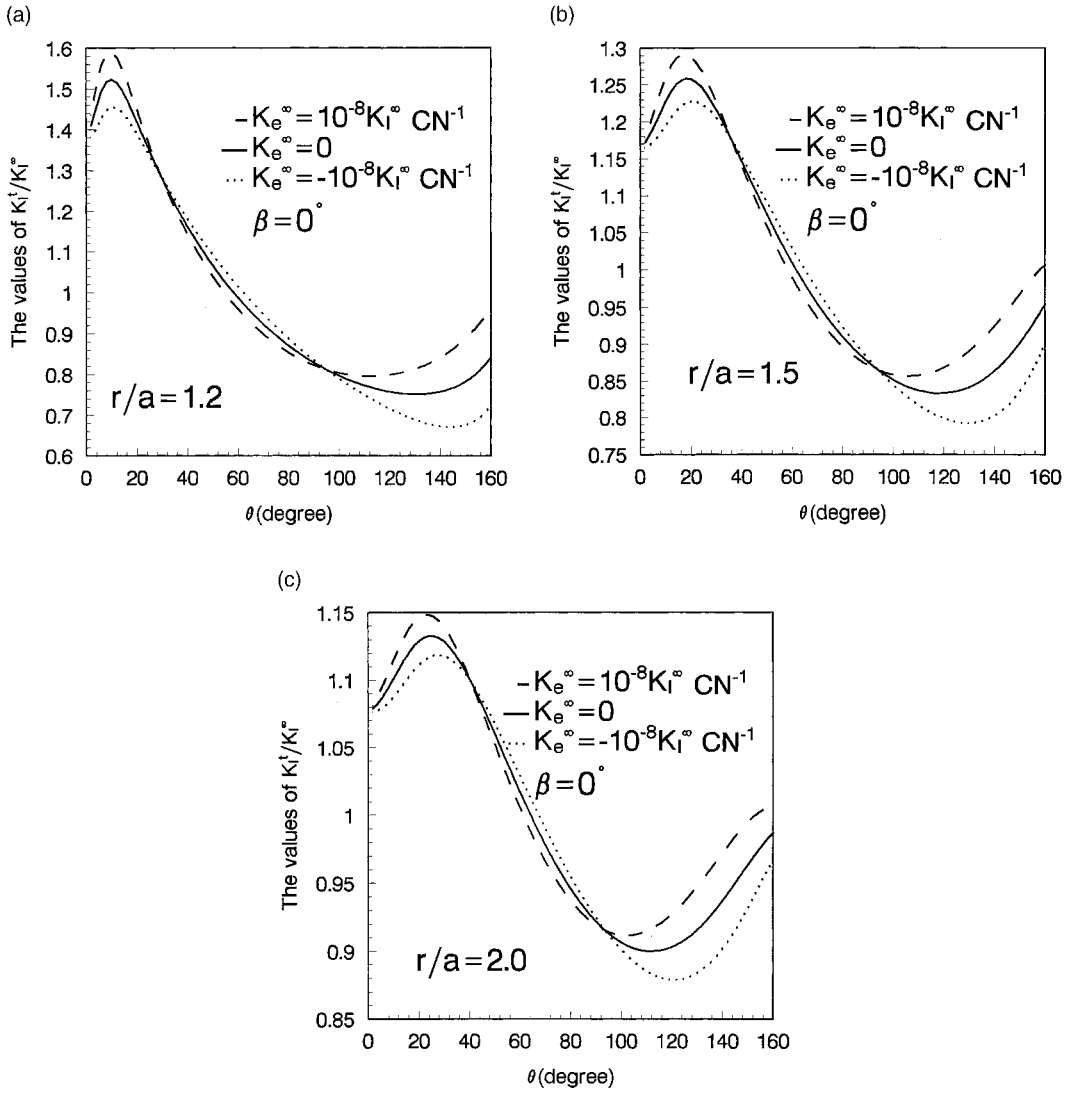

Fig. 4. The normalized stress intensity factor K_I^t/K_I^∞ vs. the angle θ: (a) $r/a = 1.2$, (b) $r/a = 1.5$ and (c) $r/a = 2.0$.

2.0, the numerical results of the normalized Mode I stress intensity K_I^t/K_I^∞ at the macrocrack tip against the angle θ are shown in Fig. 4(a)–(c). It can be found from Fig. 4 that the mechanical loading and the electric loading are really coupled to take effect on the macrocrack–microcrack interaction behavior. For example, in the range of θ smaller than 29° in Fig. 4(a), in the range of θ smaller than 34° in Fig. 4(b), and in the

range of θ smaller than 40° in Fig. 4(c), the positive electric loading leads to aiding the amplification effect ($K_I^t/K_I^\infty > 1$), while the negative electric loading leads to impeding the amplification effect. However, in the range of θ larger than 94° in Fig. 4(a) and (b), and in the range of θ larger than 93.5° in Fig. 4(c), the positive electric loading leads to impeding the shielding effect ($K_I^t/K_I^\infty < 1$), while the negative electric loading leads to aiding the shielding effect. It is also found from Fig. 4 that, in the range of θ between 29° and 94° in Fig. 4(a), in the range of θ between 34° and 94° in Fig. 4(b), and in the range of θ between 40° and 93.5° in Fig. 4(c), the positive electric loading decreases the amplification effect and increases the shielding effect; on the contrary, the negative electric loading increases the amplification and decreases the shielding effect. On the other hand, the above phenomena reveal that the microcrack shielding or amplification effect is distinctly different for the sign of the electric loading and the different microcrack location. In addition, it is obviously seen from Fig. 4 that the curves in each of the figures cross at two points at which the numerical results of the normalized Mode I stress intensity factor K_I^t/K_I^∞ are weakly dependent on the electric loading. Such specified microcrack location angles are called neutral electric loading angles (NELA) and denoted by θ_{NE} in this paper. From Fig. 4, it is known that the NELA θ_{NE} equals to about 29° and 94° for $r/a = 1.2$ (Fig. 4(a)), 34° and 94° for $r/a = 1.5$ (Fig. 4(b)), and 40° and 93.5° for $r/a = 2.0$ (Fig. 4(c)), respectively. Moreover, it can also be seen that the positive electric loading increases the maximum amplification effect and decreases the maximum shielding effect, while the negative electric loading decreases the maximum amplification effect and increases the maximum shielding effect.

Then, consider an interface macrocrack and an arbitrarily oriented subinterface microcrack of length $2a$ as shown in Fig. 3. The numerical results of the normalized Mode I stress intensity factor K_I^t/K_I^∞ at the macrocrack tip with the variation of the microcrack orientation angle β are shown in Fig. 5(a)–(c) for $\theta = 60°$, 90°, and 120°, respectively. It can be found from Fig. 5(a) that the positive electric loading always increases the shielding effect and decreases the amplification effect, while the negative electric loading always decreases the shielding effect and increases the amplification effect. Moreover, no neutral electric loading angle occurs in the whole curves (Fig. 5(a)). From Fig. 5(b) and (c), it can be found that in the range of β between 0° and 130°, and between 168° and 180° in Fig. 5(b), and in the range of β between 33° and 73° in Fig. 5(c), the positive electric loading leads to impeding the amplification effect and aiding the shielding effect, while the negative electric loading leads to aiding the amplification effect and impeding the shielding effect. However, in the range of β between 130° and 168° in Fig. 5(b), in the range of β between 0° and 33° and in the range of β between 73° and 180° in Fig. 5(c), the positive electric loading weakens the shielding effect, and be contrary to this the negative electric loading strengthens the shielding effect. Furthermore, there exist two neutral electric loading angles β_{NE} in Fig. 5(b) and (c). β_{NE} equals to about 130° and 168° when $\theta = 90°$, and β_{NE} equals to about 33° and 73° when $\theta = 120°$. Besides these, it can also be found that the electric loading has little influence on the maximum amplification angle, while it has a remarkable influence on the maximum shielding angle.

Furthermore, consider an interface macrocrack and two subinterface microcracks of the same length $2a$ shown in Fig. 6 where r_1 and r_2 denote the distances between the macrocrack tip and the centers of the two subinterface microcracks, respectively, θ_1 and θ_2 are the including angles between r_1, r_2 and the x-axis, β_1 and β_2 represent the orientation angles of the two subinterface microcracks. Taking $r_1/a = 1.5$, $r_2/a = 2.5$, $\theta_1 = 45°$, $\theta_2 = 135°$, and $\beta_2 = 0°$, the computed values of K_I^t/K_I^∞ with the variation of angle β_1 are shown in Fig. 7. It is found from Fig. 7 that in the range of β_1 between 0° and 110°, the influence of the electric loading on the macrocrack–microcrack interaction behavior is relatively large, i.e. the positive electric loading increases the amplification effect and decreases the shielding effect, while the negative electric loading decreases the amplification effect and increases the shielding effect. However, when the value of β_1 becomes larger than 110°, the interaction curves obtained under compound mechanical-electric loading condition (see the dotted lines and the imaginary line in the figure) nearly coincide with that derived under purely mechanical loading condition (see the real line in the figure); in other words, the numerical results of K_I^t/K_I^∞ are weakly dependent on the electric loading.

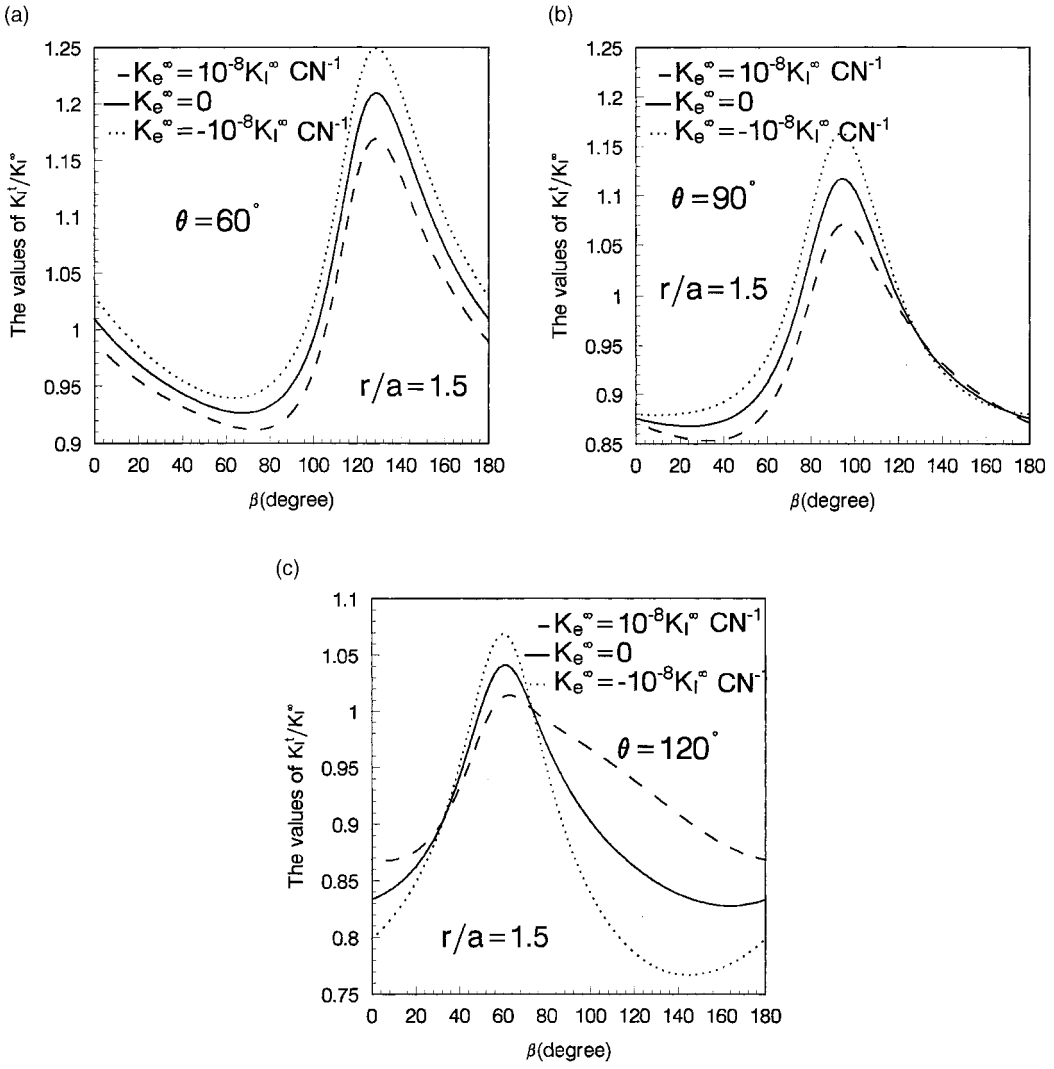

Fig. 5. The normalized stress intensity factor K_I^t/K_I^∞ vs. the angle β: (a) $\theta = 60^\circ$, (b) $\theta = 90^\circ$ and (c) $\theta = 120^\circ$.

5. Conclusions

From the above discussion, the following conclusions could be obtained:

1. The PTEDM is really effective to solve the interaction problem between a semi-infinite interface crack and subinterface cracks in metal/ piezoelectric bimaterials.
2. The mechanical loading and the electric loading are coupled to take effect on the macrocrack–microcrack interaction in metal/piezoelectric bimaterials.
3. The electric loading can bring remarkable influence on the interaction effect of a semi-infinite interface crack and multiple subinterface microcracks in metal/piezoelectric bimaterials. Influences of electric loading on microcrack shielding or amplification effect are substantially dependent on the sign of the electric loading and the geometry of the microcrack arrangement.

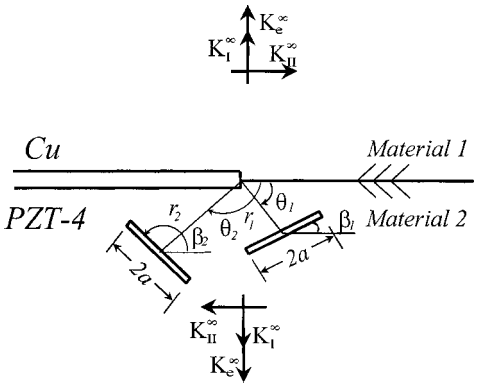

Fig. 6. An interface macrocrack and two subinterface microcracks.

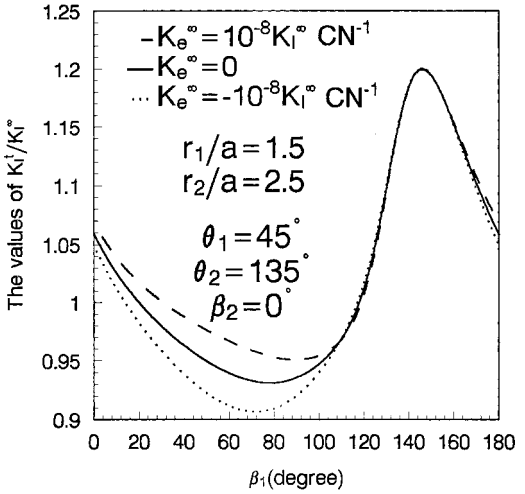

Fig. 7. The normalized stress intensity factor K_I^1/K_I^∞ vs. the angle β_1.

4. The influences of the positive electric loading on the amplification effect and the shielding effect are opposite to those of the negative electric loading.
5. The NELA are dependent on the configuration of subinterface microcracks.

Acknowledgements

This work was supported by the Chinese National Natural Science Foundation and the Doctorate Foundation of Xi'an Jiaotong University.

References

Chen, Y.H., Han, J.J., 1999a. Macrocrack–microcrack interaction in piezoelectric material, Part I: Basic formulations and J-analysis. J. Appl. Mech. 66, 514–521.

Chen, Y.H., Han, J.J., 1999b. Macrocrack–microcrack interaction in piezoelectric material, Part II: Numerical results and discussions. J. Appl. Mech. 66, 522–527.

Chen, Y.H., Hasebe, N., 1994. Interaction between a main-crack and a parallel microcrack in an orthotropic plane elastic solid. Int. J. Solids Struct. 31, 1877–1890.

Horii, H., Nemat-Nasser, S., 1985. Elastic field of interacting inhomogeneities. Int. J. Solids Struct. 21, 731–745.

Hori, M., Nemat-Nasser, S., 1987. Interacting micro-cracks near the tips in the process zone of a macro-crack. J. Mech. Phys. Solids 35, 601–629.

Kuo, C.M., Barnett, D.M., 1991. In modern theory of anisotropic elasticity and application. In: Wu, J.J., Ting T.C.T., Barnett D.M. (Eds.), SIAM Proceedings Series, Philadelphia, PA. pp. 30–50.

Pak, Y.E., 1992. Linear electric-elastic fracture mechanics of piezoelectric materials. Int. J. Fract. 54, 79–100.

Park, S.B., Carman, G.P., 1997. Minimizing stress levels in piezoelectric media containing elliptical voids. J. Appl. Mech. 64, 466–470.

Park, S.B., Sun, C.T., 1995a. Fracture criteria for piezoelectric ceramics. J. Am. Ceram. Soc. 78 (6), 1475–1480.

Park, S.B., Sun, C.T., 1995b. Effect of electric field on fracture of piezoelectric ceramics. Int. J. Fract. 70, 203–216.

Parton, V.Z., 1976. Fracture mechanics of piezoelectric materials. Acta Astronautica 3, 671–683.

Shindo, Y., Ozawa, E., 1990. Dynamic analysis of a cracked piezoelectric material. In: Hsieh, R.K.T. (Ed.), Mechanical modelling of new electromagnetic materials. Elsevier, Amsterdam.

Sosa, H., 1992. On the fracture mechanics of piezoelectric solids. Int. J. Solids Struct. 29, 2613–2622.

Sosa, H., Pak, Y.E., 1990. Three dimensional eigenfunction analysis of a crack in a piezoelectric material. Int. J. Solids Struct. 26, 1–15.

Suo, Z.G., 1990. Singularities, interfaces and cracks in dissimilar anisotropic media. Proc. R. Soc. Lond. A 427, 331–358.

Suo, Z.G., Huo, K.M., Barnett, D.M., Willis, J.R., 1992. Fracture mechanics for piezoelectric ceramics. J. Mech. Phys. Solids 40 (4), 739–765.